Title

Ionizing radiation induces mitochondrial ROS production accompanied by upregulation of mitochondrial electron transport chain function and mitochondrial content under control of the cell cycle checkpoint

Authors

Tohru Yamamori[a], Hironobu Yasui[a], Masayuki Yamazumi[a], Yusuke Wada[a], Yoshinari Nakamura[a], Hideo Nakamura[b], Osamu Inanami[a]

Affiliations

[a]Laboratory of Radiation Biology, Department of Environmental Veterinary Sciences, Graduate School of Veterinary Medicine, Hokkaido University, Sapporo 060-0818, Japan

[b]Department of Humanities and Regional Sciences, Hokkaido University of Education Hakodate, Hakodate 040-8567, Japan

Correspondence author: Osamu Inanami, Kita 18, Nishi 9, Kita-ku, Sapporo 060-0818, Japan.
Tel: +81-11-706-5235; Fax: +81-11-706-7373; E-mail: inanami@vetmed.hokudai.ac.jp

Abstract

While ionizing radiation (Ir) instantaneously causes the formation of water radiolysis products that contain some reactive oxygen species (ROS), ROS are also suggested to be released from biological sources in irradiated cells. It is now becoming clear that these secondarily generated ROS after Ir have a variety of biological roles. Although mitochondria are assumed to be responsible for this Ir-induced ROS production, it remains to be elucidated how Ir triggers it. Therefore, we conducted this study to decipher the mechanism of Ir-induced mitochondrial ROS production. In human lung carcinoma A549 cells, Ir (10 Gy of X-rays) induced a time-dependent increase of the mitochondrial ROS level. Ir also increased mitochondrial membrane potential, mitochondrial respiration, and mitochondrial ATP production, suggesting upregulation of the mitochondrial electron transport chain (ETC) function after Ir. Although we found that Ir slightly enhanced mitochondrial ETC complex II activity, the complex II inhibitor 3-nitropropionic acid failed to reduce Ir-induced mitochondrial ROS production. Meanwhile, we observed that the mitochondrial mass and mitochondrial DNA level were upregulated after Ir, indicating that Ir increased mitochondrial content of the cell. Because irradiated cells are known to undergo cell cycle arrest under control of the checkpoint mechanisms, we examined the

relationships between the cell cycle and mitochondrial content and cellular oxidative stress level. We found that the cells in the G2/M phase had a higher mitochondrial content and cellular oxidative stress level than cells in the G1 or S phase, regardless of whether the cells were irradiated. We also found that Ir-induced accumulation of the cells in the G2/M phase led to an increase of cells with a high mitochondrial content and cellular oxidative stress level. This suggested that Ir upregulated mitochondrial ETC function and mitochondrial content, thereby resulting in mitochondrial ROS production and that Ir-induced G2/M arrest contributed to the increase of the mitochondrial ROS level by accumulating cells in the G2/M phase.

Keywords: ionizing radiation, mitochondrial ROS, electron transport chain, cell cycle

Introduction

Ionizing radiation (Ir) initially causes ionization and excitation of water, leading to the formation of water radiolysis products such as hydrated electron (e_{aq}^-), ionized water (H_2O^+), hydroperoxyl radical ($HO_2^\bullet$), hydroxyl radical ($^\bullet OH$), hydrogen radical ($H^\bullet$), hydrogen peroxide (H_2O_2) in a very short period of time (~10^{-8} sec) when irradiated to a biological system [1]. Except H_2O_2, they are unstable and disappear within less than 10^{-3} sec [1]. A significant part of the initial damage done to cells by Ir is due to DNA damage, and these water radiolysis products (especially $^\bullet OH$) play an important role in this process [2, 3]. Some of water radiolysis products such as $^\bullet OH$ and $HO_2^\bullet$ are also called reactive oxygen species (ROS), a group of chemically reactive molecules containing oxygen. ROS have been suggested to be involved in a variety of biological processes ranging from cell proliferation to carcinogenesis. The main ROS that have marked biological effects are superoxide radical ($O_2^{\bullet -}$), H_2O_2, $^\bullet OH$, peroxyl radical ($ROO^\bullet$), alkyl hydroperoxide (ROOH) and singlet oxygen ($^1O_2$) [4]. Most ROS are labile and dissipate quickly except H_2O_2 and ROOH, which are relatively stable. When irradiated to cells, not only Ir leads to the generation of ROS derived from water radiolysis, it has been shown that Ir increases the intracellular level of ROS including $O_2^{\bullet -}$ several hours after its exposure [5, 6],

indicating that Ir also stimulates ROS production derived from biological sources. It is becoming clear that the secondarily generated ROS after Ir have a variety of biological roles. These include apoptotic signaling, genomic instability after Ir, and radiation-induced bystander effects [7-12]. These effects ultimately have an impact on cellular integrity and survival. Therefore, it is of considerable significance to determine the mechanism underlying the Ir-induced cellular ROS production from the aspect of radiation biology.

Thus far, there is conflicting evidence on the source of the secondarily generated ROS after Ir. Though it is reported that NADPH oxidase is involved in Ir-induced ROS production [5, 13], several studies, including ours, suggested that mitochondria are responsible for it [7, 14, 15]. However, it remains unclear how Ir induces ROS production from mitochondria. In general, it has been postulated that electron leakage from mitochondrial electron transport chain (ETC) complexes to molecular oxygen causes the generation of $O_2^{\bullet-}$ and its derivative ROS (such as H_2O_2 and $^{\bullet}OH$) in mitochondria (hereafter "mitochondrial ROS") [16-18]. Mitochondrial respiration for ATP production leads to mitochondrial ROS production, and 0.12-2% of O_2 incorporated for respiration is estimated to go to $O_2^{\bullet-}$ under *in vitro* conditions [16]. ETC complex inhibitors such as rotenone and antimycin A potentiate mitochondrial $O_2^{\bullet-}$

production by enhancing this electron leakage, indicating that the electron flow through ETC strongly influences mitochondrial ROS production [16, 19].

Although it has been suggested that Ir promotes mitochondrial ROS production, it remains to be elucidated how Ir triggers it. Therefore, we conducted this study to decipher the mechanism of Ir-induced mitochondrial ROS production.

Materials and Methods

Reagents

2',7'-Dichlorofluorescein diacetate (DCFDA) and 3-nitropropionic acid (3-NP) were obtained from Sigma-Aldrich (St. Louis, MO). Tetramethylrhodamine methyl ester (TMRM) and MitoSOX Red (MSR) were purchased from Invitrogen (Carlsbad, CA). ATP assay kits were from TOYO B-Net Co. (Tokyo, Japan). Nuclear-ID Red DNA stain was obtained from Enzo Life Sciences (Farmingdale, NY). Rotenone, carbonyl cyanide m-chlorophenyl hydrazone (CCCP), oligomycin and other reagents were obtained from Wako Pure Chemical Co. (Osaka, Japan).

Cell culture and treatment

Human lung carcinoma A549 cells were maintained in RPMI1640 medium (Invitrogen) supplemented with 10% fetal bovine serum (RPMI1640/10% FBS) at 37˚C in 5% CO_2. Human cervical carcinoma

HeLa S3 cells were grown as suspension cultures in Joklik's-MEM (Sigma-Aldrich) containing 10% FBS at 37°C in 5% CO_2. X-irradiation was performed with an X-ray generator (Shimadzu HF-350; Kyoto, Japan) and the dose rate was 3.9 Gy/min at 200 kVp, 20 mA with a 1.0 mm aluminum filter, which was determined using Fricke's chemical dosimeter. Drugs were added immediately after irradiation, with incubation for the indicated times.

Cellular oxidative stress levels and mitochondrial ROS production

The fluorescent probe DCFDA was used for the assessment of cellular oxidative stress levels [20, 21]. Cells were incubated with RPMI1640/10% FBS containing 10 μM DCFDA for 30 min at 37°C. Then they were trypsinized and washed twice with PBS(-). After resuspending the cells in serum-free RPMI1640 medium, they were analyzed using an EPICS XL flow cytometer (Beckman Coulter, Fullerton, CA). The mean DCFDA fluorescent intensity of each sample was normalized to that of a control sample to calculate the relative DCFDA intensity.

Another fluorescent probe MSR was used for the assessment of mitochondria-derived $O_2^{\bullet-}$ and other oxidants (such as H_2O_2 and $^{\bullet}OH$) [20, 22, 23]. Cells were incubated with RPMI1640/10% FBS containing 2 μM MSR for 30 min at 37°C. Then they were trypsinized and washed twice with PBS(-). After resuspending

them in serum-free RPMI1640 medium, the cells were analyzed as described above.

Mitochondrial membrane potential

The fluorescent probe TMRM was used for the assessment of mitochondrial membrane potential [22]. Cells were incubated in RPMI1640/10% FBS containing 20 nM TMRM for 30 min at 37°C. Then they were trypsinized and washed twice with PBS(-). After resuspending the cells in serum-free RPMI1640 medium, they were analyzed using an EPICS XL flow cytometer. The mean TMRM fluorescent intensity of each sample was normalized to that of a control sample to calculate the relative TMRM intensity.

Oxygen consumption analysis by polarography

Cells were trypsinized and washed twice with PBS(-). Then they (5×10^6 cells) were resuspended in buffer E (0.3 M mannitol, 10 mM KCl, 5 mM $MgCl_2$, 1 mg/ml BSA, 10 mM KH_2PO_4 [pH 7.4]) and transferred to a sample chamber. Oxygen consumption by the cells was monitored using a YSI 5300 biological oxygen monitor (YSI Life Sciences, Yellow Springs, OH). Rotenone (final conc. = 2 μM) was added to the cell suspension with a microsyringe.

Measurement of oxygen consumption rate by electron spin resonance (ESR) spectroscopy

The peak-to-peak line width of the ESR spectrum of lithium 5,9,14,18,23,27,32,36-octa-*n*-butoxy-2,3-naphthalocyanine (LiNc-BuO) shows a linear response to the partial pressure of oxygen (pO_2) and has been used extensively to measure oxygen consumption *in vitro* [24, 25]. LiNc-BuO was synthesized according to the method described previously [26, 27]. At indicated periods after 10 Gy of X-irradiation, cells were collected and washed. The cells (5×10^5 cells) were suspended in 100 µl of serum-free medium containing 0.2 mg LiNc-Buo and 2% dextran to avoid sedimentation of the cells and LiNc-BuO particles. The cell suspension was immediately drawn into a glass capillary tube, which was then sealed at both ends. The ESR measurements were carried out using a JEOL-RE X-band spectrometer (JEOL, Tokyo, Japan) with a cylindrical TE011 mode cavity (JEOL). The cavity was maintained at 37˚C using a temperature controller (ES-DVT4, JEOL). Spectrometer conditions were as follows: incident microwave power, 10 mW; modulation frequency, 100 kHz; field modulation amplitude, 63 µT; and scan range, 0.5 mT. The spectral line widths were analyzed using a Win-Rad Radical Analyzer System (Radical Research, Tokyo, Japan) and converted into pO_2 values according to the following equation described by Fujii *et al.* [27].

pO_2 (mmHg) = (LW x 10-340)/10.33 (LW; ESR line width [µT])

To examine the relationship between mitochondrial respiration and cellular oxygen consumption, rotenone was added at 2 μM where indicated.

Cellular ATP content

Cellular ATP content was evaluated with the ATP assay kit according to the provider's protocol. In brief, cells were collected and resuspended in RPMI1640/10% FBS. The cells (5 x 10^3 cells/100 μl) were transferred to wells of 96-well plate, followed by the addition of ATP assay reagent (100 μl). After incubating the plate for 30 min at 25°C, chemiluminescence from each well was measured with a luminometer (Luminescencer-JNR; ATTO, Tokyo, Japan) set at 25°C.

Isolation of mitochondria

Intact mitochondria were isolated from HeLa S3 cells. At 12 h after X-irradiation, the cells were collected and resuspended in ice-cold isolation buffer (2.5 mM HEPES-KOH [pH 7.4], 70 mM sucrose, 220 mM mannitol, 1 mM EGTA). A nitrogen cell disruption vessel, model 4639 from Parr Instrument Company (Moline, IL), was used to burst cells. The cell suspension was placed into the cell disruption chamber and put under a pressure of 250 psi for 30 min at 4°C. After unbroken cells and nuclei were removed

by centrifuging the suspension at 1000 g for 10 min at 4°C, the supernatant was further centrifuged at 10,000 g for 10 min at 4°C to precipitate mitochondria. The final mitochondrial pellet was resuspended in isolation buffer and the protein concentration was determined using the Bio-Rad protein assay (Bio-Rad, Hercules, CA).

Mitochondrial ETC enzyme activities

Complex I activity was measured as the rotenone (2 µg/ml)-inhibitable rate of NADH (0.325 mM) oxidation in 25 mM KH_2PO_4 (pH 7.2), 5 mM $MgCl_2$, 2.5 mg/ml BSA, 65 µM Coenzyme Q_1 (Sigma-Aldrich), 2 µg/ml antimycin A, and 2 mM KCN. The rate of the absorbance change at 340 nm with a 425 nm reference wavelength was measured. To measure complex II activity, mitochondrial extract was incubated in a mixture of 25 mM KH_2PO_4 (pH 7.2), 20 mM sodium succinate, 5 mM $MgCl_2$, 150 µM 2,6-dichlorophenolindophenol (DCPIP), 2 mM KCN, 2 µg/ml antimycin A, and 10 µg/ml rotenone. Sixty-five µM Coenzyme Q_1 was then added to the mixture and the rate of DCPIP reduction was monitored at 600 nm with a 750 nm reference wavelength. Complex IV activity was measured by the rate of oxidation of cytochrome c (II) (15 µM) in 25 mM KH_2PO_4 (pH 7.2) and 0.45 mM n-dodecyl β-maltoside. The rate of the absorbance change at 550 nm with a 580 nm reference wavelength was measured. Complex

I+III activity was measured as the rotenone (2 μg/ml)-inhibitable rate of reduction of cytochrome c (III) (80 μM) in 50 mM KH_2PO_4 (pH 7.2), 0.2 mM NADH, and 2 mM KCN. The rate of the absorbance change at 550 nm with a 580 nm reference wavelength was read. For complex II+III activity, mitochondrial extract was incubated in a mixture of 40 mM KH_2PO_4 (pH 7.2), 20 mM sodium succinate, 0.5 mM EDTA, 2 mM KCN, and 10 μg/ml rotenone. Cytochrome c (III) (62.5 μM) was then added to the mixture and its reduction rate was monitored at 550 nm with a 580 nm reference wavelength. All mitochondrial ETC enzyme activities were normalized to the total protein amount.

Mitochondrial mass

Mitochondrial mass was measured by staining cells with a membrane potential-independent mitochondrial dye MitoTracker Green FM (Invitrogen) [22]. Cells were incubated in RPMI1640/10% FBS containing 50 nM MitoTracker Green FM for 30 min at 37°C. Then they were trypsinized and washed twice with PBS(-). After being resuspended in PBS(-), the cells were analyzed using an EPICS XL flow cytometer.

Mitochondrial DNA content

Mitochondrial DNA (mtDNA) content was determined as a marker for mitochondrial density using quantitative RT-PCR as

previously reported [28, 29]. In brief, total DNA was isolated from the cells using a FastPure DNA kit (TAKARA BIO, Shiga, Japan) according to the manufacturer's instructions. To evaluate the mtDNA content, the relative amounts of D-loop and cytochrome c oxidase subunit II (COXII) (mtDNA-encoded) were determined by the ΔΔCt method using β2-microglobulin (β2M) (nuclear DNA-encoded) as an internal control.

Simultaneous flow cytometric analysis of cell cycle/mitochondrial content and cell cycle/cellular oxidative stress levels using a double-staining technique

For simultaneous analysis of the cell cycle and mitochondrial content, we used two fluorescent probes, Nuclear-ID Red and MitoTracker Green for staining the nuclear DNA and mitochondrial membrane, respectively. After irradiated cells were trypsinized and washed with PBS(-), they were incubated with serum-free RPMI1640 containing 20 μM Nuclear-ID Red and 40 nM MitoTracker Green for 30 min at 37°C. The cells were then analyzed using an EPICS XL flow cytometer. MitoTracker Green fluorescence of the cell fraction corresponding to the G1, S, and G2/M phases was analyzed to determine the mitochondrial content of the cells in each cell cycle phase. The mean MitoTracker Green fluorescence intensity of each sample was normalized to that of a control sample to calculate relative

MitoTracker Green intensity. For simultaneous analysis of the cell cycle and cellular oxidative stress levels, we applied the method described above using 10 μM DCFDA as a probe for the cellular oxidative stress instead of MitoTracker Green.

Statistical analysis

All results were expressed as means ± SE of at least three separate experiments. Statistical analyses were performed with Student's *t*-test. The minimum level of significance was set at $p < 0.05$.

Results

Ionizing radiation induces mitochondrial ROS production

We first examined the cellular oxidative stress levels in human lung carcinoma A549 cells after Ir using the fluorescent probe DCFDA and a flow cytometer [20, 21]. When A549 cells were incubated for 12 h after X-irradiation (10 Gy), they became more oxidized than the cells collected immediately after irradiation (Fig. 1A). As shown in Fig. 1B, DCFDA fluorescence intensity in A549 cells gradually increased after Ir, peaked at 12 h, and declined at 24 h, consistent with our previous report [7].

To test if Ir stimulated mitochondrial ROS production, we analyzed it using the fluorescent probe MSR and a flow cytometer [20, 22, 23]. Cells collected 12 h after X-irradiation

exhibited higher MSR fluorescence intensity than the cells collected immediately after irradiation (Fig. 1C). As shown in Fig. 1D, Ir increased MSR fluorescence intensity in a time-dependent manner. In addition, we examined mitochondrial ROS production after Ir in various cell lines (HeLa, MKN45, MeWo, NIH3T3) and found that Ir facilitated it in all cell lines tested (data not shown). These results indicated that Ir induced cellular oxidative stress and that mitochondrial ROS were, at least in part, responsible for it.

Ionizing radiation increases mitochondrial membrane potential

We next evaluated the mitochondrial membrane potential after Ir using the fluorescent probe TMRM and a flow cytometer [22]. When A549 cells were incubated for 12 h after Ir, they showed higher TMRM fluorescence intensity than the cells collected immediately after irradiation (Fig. 2A). As shown in Fig. 2B, the TMRM intensity in A549 cells was time-dependently increased up to 48 h after Ir. To confirm that this change was caused by the increase of mitochondrial membrane potential *per se*, we tested the effect of an uncoupling agent CCCP on TMRM fluorescence intensity. As shown in Fig. 2C, the TMRM intensity was increased after Ir exposure and it was dissipated by the CCCP treatment. Therefore, these results demonstrated that the mitochondrial membrane potential was increased after Ir.

Ionizing radiation promotes mitochondrial respiration

We next investigated if Ir affected cellular respiration. Cellular oxygen consumption was monitored using a standard polarographic technique with a Clark-type oxygen electrode. As shown in Fig. 3A, the oxygen concentration in the sample chamber stayed the same in the absence of cells (buffer only). When cells were loaded in the chamber, the oxygen concentration decreased at a constant rate. It was completely inhibited by the addition of rotenone, indicating that the reduction in the oxygen concentration was attributable to mitochondrial respiration. When A549 cells were X-irradiated, they showed higher respiratory activity than the cells collected immediately after irradiation, with a 1.6-fold increase (Figs. 3A and 3B).

To support this observation, we further analyzed the cellular oxygen consumption rate by ESR spectrometry using LiNc-BuO as an oxygen sensing probe. The peak-to-peak line width of the ESR spectrum of LiNc-BuO particles broadens as the pO_2 increases [26]. When non-irradiated A549 cells were mixed with LiNc-BuO particles and the ESR measurement was performed, the ESR spectra were sharpened in a time-dependent manner, indicating the cellular oxygen consumption (Fig. 4A; left). The sharpening of the spectra was observed more rapidly in X-irradiated cells (Fig 4A; right), suggesting that Ir

stimulated cellular oxygen consumption. After the line width of the spectrum was converted into a pO_2 value as described in *Materials and Methods*, the pO_2 was plotted as a function of time (Fig. 4B) and the cellular oxygen consumption rate was calculated (Fig. 4C). Figures 4B and 4C demonstrate that Ir elevated cellular oxygen consumption up to 12 h after irradiation, followed by a decrease at 24 h. These results were consistent with the data obtained by polarography (Figs. 3A and 3B). Furthermore, we examined cellular oxygen consumption after Ir in various cell lines (HeLa, MKN45, MeWo, NIH3T3), and found that Ir facilitated it in all cell lines tested (data not shown).

We then evaluated the effect of rotenone on the Ir-induced cellular oxygen consumption to determine whether mitochondrial respiration was involved in it. As shown in Figs. 4D and 4E, Ir stimulated cellular oxygen consumption and rotenone suppressed not only basal cellular oxygen consumption but also Ir-stimulated cellular oxygen consumption. These results indicated that mitochondrial respiration was responsible for the basal and Ir-induced cellular oxygen consumption.

Ionizing radiation promotes ATP production

Because higher mitochondrial respiration has been linked to the higher cellular energy production, we hypothesized that the upregulation of mitochondrial respiration by Ir led to the

upregulation of ATP production. To test this hypothesis, we measured cellular ATP content using a commercially available assay kit. As shown in Fig. 5A, Ir resulted in a time-dependent increase of cellular ATP content up to 24 h after irradiation. When the mitochondrial ATP synthase (F_0/F_1-ATPase) inhibitor oligomycin was applied to the cells after Ir, it reduced the cellular ATP content stimulated by Ir in a concentration-dependent manner without affecting the basal cellular ATP level (Fig. 5B). These data suggested that Ir facilitated mitochondrial energy production activity.

ETC enzyme activities are unaffected by ionizing radiation and are not associated with the mitochondrial ROS production

These data prompted us to examine if any of the mitochondrial ETC enzyme activities were affected by Ir. To this end, mitochondria were isolated from irradiated and non-irradiated HeLa S3 cells and ETC enzyme activities were analyzed. While the activities of complex I+III, complex IV, and complex I were almost same with or without Ir, the activities of complex II+III and complex II were slightly increased after Ir although they are not statistically significant (Table 1). This result implied that, at the mitochondrial level, only complex II activity was upregulated by Ir among all ETC enzymes evaluated.

To investigate if the complex II activity elevated by Ir

was involved in the Ir-induced mitochondrial ROS production, we tested the effect of the complex II inhibitor 3-NP in A549 cells. As shown in Fig. 6, Ir promoted mitochondrial ROS production measured by MSR fluorescence, and we did not observe any substantial effect of 3-NP treatment on it. These results suggested that the upregulation of complex II activity by Ir was not associated with the Ir-induced mitochondrial ROS production.

Ir-induced cell cycle regulation affects mitochondrial content and intracellular ROS level

Because the intracellular ROS level is reported to be affected by mitochondrial content of the cell [30], we then examined whether Ir affected mitochondrial content in cells. We evaluated mitochondrial content using two methods, mitochondrial mass measured by MitoTracker Green staining [22] and mtDNA content measured by quantitative PCR. It was demonstrated that Ir increased the mitochondrial mass (Fig. 7A) as well as mtDNA content (Fig. 7B) in A549 cells, indicating that Ir increased the mitochondrial content of the cell.

Recent studies have shown that mitochondrial content can be influenced by the cell cycle of the host cell [31, 32]. Because tumor cells are known to accumulate in the G2 phase of the cell cycle after Ir exposure [33], we further investigated whether

the cell cycle arrest triggered by Ir was involved in the Ir-induced upregulation of the mitochondrial content and cellular oxidative stress. A technique for double-staining of live cells with Nuclear-ID Red and MitoTracker Green for staining nuclear DNA and mitochondrial membrane, respectively, enabled us to analyze the mitochondrial content of the cell fraction in specific phases of the cell cycle. Figure 8A shows typical flow cytometric profiles in A549 cells after Ir analyzed by Nuclear-ID Red fluorescence from double-stained cells. It was demonstrated that the number of cells in the G2/M phase time-dependently increased up to 12 h after Ir. MitoTracker Green fluorescence of the cell fraction corresponding to the G1, S, and G2/M phases was analyzed to determine the mitochondrial content of the cells in each phase of the cell cycle. The flow cytometric profiles of MitoTracker Green fluorescence from each cell cycle fraction at the indicated times after Ir are overlaid and shown in Fig. 8B, which demonstrates that the cell fraction in the G2/M phase had the highest mitochondrial content, followed by those in the S phase and G1 phase. Moreover, it also shows that Ir-induced accumulation of the cells in the G2/M phase resulted in an increase of cells with a high mitochondrial content. This was confirmed by the graph in Fig. 8C, which demonstrates the relative mitochondrial content during the cell cycle after Ir.

The mitochondrial content was increased in the order G1, S, G2/M regardless of the time after irradiation.

We then analyzed the cellular oxidative stress levels during the cell cycle by applying the same method using DCFDA as a probe for the cellular oxidative stress instead of MitoTracker Green. We could not use MSR in this system because it has excitation/emission characteristics similar to Nuclear-ID Red. Figures 9A and 9B demonstrate that, similar to the results in Fig. 8: 1) Ir induced cell cycle arrest in the G2/M phase; 2) the cell fraction in the G2/M phase had the highest cellular oxidative stress level, followed by those in the S phase and G1 phase; 3) consequently, Ir-induced accumulation of the cells in the G2/M fraction resulted in an increase of the cells with a high cellular oxidative stress level. Figure 9C shows that the cellular oxidative stress level was increased in the order G1, S, G2/M regardless of the time after irradiation.

Taken together, these data showed that, regardless of whether cells were irradiated, the cells in the G2/M phase had more mitochondria and a higher cellular oxidative stress level than those in the G1 or S phase. Because Ir caused accumulation of cells in the G2/M phase, it led to the increase of the cells with a high mitochondrial content and a high cellular oxidative stress level.

Discussion

The aim of the present study was to determine how Ir triggers mitochondrial ROS production. Our results demonstrated that Ir increased mitochondrial membrane potential (Fig. 2), mitochondrial respiration (Figs. 3 and 4), and mitochondrial ATP production (Fig. 5). These data suggested that Ir upregulated mitochondrial ETC function, consistent with reports showing similar data [34, 35]. Meanwhile, ETC enzyme activities were unchanged after Ir except for complex II (Table 1). This finding was inconsistent with reports showing that Ir caused no change [36] or reduced [37] ETC enzyme activities. The difference of the assay system utilized by those groups and us might explain this discrepancy. However, further studies will be necessary to determine the effect of Ir on ETC enzymes. In the present study, mitochondrial ROS production was accompanied by increased mitochondrial membrane potential, enhanced mitochondrial respiration, and maintained ETC enzyme activities. This suggested that mitochondrial ROS were released from functionally active mitochondria. While it is often considered that impairment of ETC function leads to mitochondrial ROS production [38], Kadenbach and other groups have reported that mitochondrial $O_2^{\bullet -}$ production increases exponentially as mitochondrial membrane potential increases,

especially when it exceeds roughly 140 mV [39-42]. This level of mitochondrial hyperpolarization can be achieved by sustained mitochondrial respiration in the absence of ADP (state 4 respiration) [39]. Hence, it is possible that Ir elicited state 4 respiration and mitochondrial hyperpolarization, resulting in mitochondrial ROS production. However, the increased mitochondrial ATP production that we observed in this study has not been linked to state 4 respiration. Thus further investigation is required to fully understand the relationship between mitochondrial ETC function and ROS production after Ir.

Moreover, we found that Ir increased mitochondrial content (Fig. 7). Nugent *et al.* demonstrated that Ir increased mitochondrial mass [43], and other groups observed increased mtDNA after Ir [37, 44]. These reports are in line with the results shown in the present study. There are two possible mechanisms to explain these events. One is cell cycle-dependent oscillations of mitochondrial content of the cell as will be discussed later, and the other is the upregulation of mitochondrial biogenesis. The increase of mtDNA content after Ir (Fig. 7B) indicates the upregulation of mitochondrial biogenesis. However, the increase of mtDNA content occurred later than that of mitochondrial mass (Fig. 7A). Therefore, it suggests that Ir-induced mitochondrial biogenesis could be an event that takes place independently of the change of

mitochondrial mass, or a secondary event caused by the change of mitochondrial mass.

In the present study, we observed the cell cycle-dependent change of mitochondrial content (Fig. 8). Other groups also have demonstrated that mitochondrial content of the cell peaks in the G2/M phase during the cell cycle [31, 45, 46]. Furthermore, these studies also reported that the increase of the intracellular ROS level is accompanied by an increase of mitochondrial content during the cell cycle, assisting our results. Therefore, it is likely that this cell cycle-dependent oscillation of the mitochondrial mass and cellular oxidative stress level is a common feature of mammalian cells.

It is noteworthy that Ir-induced G2/M arrest led to a sustained increase of cells with elevated mitochondrial content and a higher cellular oxidative stress level, presumably thereby resulting in an increase of the oxidative stress level in the whole population of the cells after irradiation. To the best of our knowledge, this is the first report suggesting that Ir-induced cell cycle arrest is involved in the increase of the cellular/mitochondrial ROS level after irradiation. Under this scenario, cells under G2/M arrest are expected to have higher mitochondrial membrane potential, mitochondrial respiration and cellular ATP level than non-irradiated cells. In fact, cell cycle-dependent oscillation of mitochondrial membrane

potential and its elevation in the G2/M phase have been reported [31, 46]. We also observed that cells in the G2/M phase had higher mitochondrial membrane potential, which was sustained after Ir (Yamamori T *et al.*, unpublished data). Recently, Kobashigawa *et al.* elegantly demonstrated that Ir-induced mitochondrial fission was essential for mitochondrial ROS production after Ir [47]. Furthermore, Mitra and colleagues reported that mitochondrial fission was increased in the G2/M phase and cells arrested in the G2/M phase by nocodazole exhibited the greatest mitochondrial fission [32]. Taking into account these findings, it might be possible that Ir-induced G2/M arrest leads to mitochondrial fission, followed by the consequential production of mitochondrial ROS.

In addition, we would like to emphasize here that Ir-induced cell cycle regulation also affect the oxidative stress that cells receive. As demonstrated in Fig. 9, cells in the G2/M phase have a higher cellular oxidative stress level than cells in other cell cycle phases. Whereas the G2/M phase lasts 5 h in non-irradiated HeLa cells, it becomes about 3 times longer after their exposure to Ir [48, 49]. Because Ir-induced G2/M arrest increases not only the length of the G2/M phase but also the number of cells in the G2/M phase, this implies that irradiated cells undergo substantial oxidative stress due to Ir-induced cell cycle arrest. Because it is widely accepted that

oxidative stress plays an important role in biological responses after Ir, Ir-induced G2/M arrest could participate in them via the elevation of oxidative stress.

In conclusion, we hypothesize the mechanism of Ir-induced mitochondrial ROS production to be as follows: in proliferating cells, the mitochondrial content, mitochondrial ETC function and mitochondrial ROS level oscillate in a cell cycle-dependent manner, and all parameters peak in the G2/M phase during the cell cycle; cells exposed to Ir accumulate in the G2/M phase under the control of the G2/M checkpoint, resulting in a corresponding increase of the mitochondrial content and mitochondrial ROS level. Although we assume that this mechanism is primarily responsible for Ir-induced mitochondrial ROS production, it is possible that concomitant events induced by Ir such as mitochondrial fission and/or a change in the ETC function play a role in mitochondrial ROS production in concert with the cell cycle-regulated mechanism. Thus further investigation is required to determine whether Ir-induced mitochondrial ROS production can be explained solely by the cell cycle-regulated mechanism, or other factors are involved in it.

Acknowledgments

This work was supported, in part, by Grants-in-Aid for Basic Scientific Research from the Ministry of Education, Culture, Sports, Science and Technology, Japan (No. 21658106, No. 21380185 [O.I.] and No. 21780267 [T.Y.]), and by the Akiyama Life Science Foundation (T.Y. and H.Y.).

Abbreviations

β2M, β2-microglobulin; CCCP, carbonyl cyanide m-chlorophenyl hydrazine; COXII, cytochrome c oxidase subunit II; DCFDA, 2',7'-dichlorofluorescein diacetate; DCPIP, 2,6-dichlorophenolindophenol; ESR, electron spin resonance; ETC, electron transport chain, Ir, ionizing radiation; LiNc-BuO, lithium 5,9,14,18,23,27,32,36-octa-n-butoxy-2,3-naphthalocyanine; mtDNA, mitochondrial DNA; MSR, MitoSOX Red; 3-NP, 3-nitropropionic acid; ROS, reactive oxygen species; TMRM, tetramethylrhodamine methyl ester

References

[1] Riley, P. A. Free radicals in biology: oxidative stress and the effects of ionizing radiation. *Int J Radiat Biol* **65**:27-33; 1994.

[2] Wallace, S. S. Enzymatic processing of radiation-induced free radical damage in DNA. *Radiat Res* **150**:S60-79; 1998.

[3] Ward, J. F. DNA damage produced by ionizing radiation in mammalian cells: identities, mechanisms of formation, and reparability. *Prog Nucleic Acid Res Mol Biol* **35**:95-125; 1988.

[4] Chance, B.; Sies, H.; Boveris, A. Hydroperoxide metabolism in mammalian organs. *Physiol Rev* **59**:527-605; 1979.

[5] Tateishi, Y.; Sasabe, E.; Ueta, E.; Yamamoto, T. Ionizing irradiation induces apoptotic damage of salivary gland acinar cells via NADPH oxidase 1-dependent superoxide generation. *Biochem Biophys Res Commun* **366**:301-307; 2008.

[6] Chen, Q.; Chai, Y. C.; Mazumder, S.; Jiang, C.; Macklis, R. M.; Chisolm, G. M.; Almasan, A. The late increase in intracellular free radical oxygen species during apoptosis is associated with cytochrome c release, caspase activation, and mitochondrial dysfunction. *Cell Death Differ* **10**:323-334; 2003.

[7] Ogura, A.; Oowada, S.; Kon, Y.; Hirayama, A.; Yasui, H.; Meike, S.; Kobayashi, S.; Kuwabara, M.; Inanami, O. Redox regulation in radiation-induced cytochrome c release from mitochondria of human lung carcinoma A549 cells. *Cancer Lett*

277:64-71; 2009.

[8] Inanami, O.; Takahashi, K.; Kuwabara, M. Attenuation of caspase-3-dependent apoptosis by Trolox post-treatment of X-irradiated MOLT-4 cells. *Int J Radiat Biol* **75:**155-163; 1999.

[9] Tominaga, H.; Kodama, S.; Matsuda, N.; Suzuki, K.; Watanabe, M. Involvement of reactive oxygen species (ROS) in the induction of genetic instability by radiation. *J Radiat Res (Tokyo)* **45:**181-188; 2004.

[10] Chen, S.; Zhao, Y.; Zhao, G.; Han, W.; Bao, L.; Yu, K. N.; Wu, L. Up-regulation of ROS by mitochondria-dependent bystander signaling contributes to genotoxicity of bystander effects. *Mutat Res* **666:**68-73; 2009.

[11] Kim, G. J.; Fiskum, G. M.; Morgan, W. F. A role for mitochondrial dysfunction in perpetuating radiation-induced genomic instability. *Cancer Res* **66:**10377-10383; 2006.

[12] Maguire, P.; Mothersill, C.; McClean, B.; Seymour, C.; Lyng, F. M. Modulation of radiation responses by pre-exposure to irradiated cell conditioned medium. *Radiat Res* **167:**485-492; 2007.

[13] Liu, Q.; He, X.; Liu, Y.; Du, B.; Wang, X.; Zhang, W.; Jia, P.; Dong, J.; Ma, J.; Li, S.; Zhang, H. NADPH oxidase-mediated generation of reactive oxygen species: A new mechanism for X-ray-induced HeLa cell death. *Biochem Biophys Res Commun* **377:**775-779; 2008.

[14] Leach, J. K.; Van Tuyle, G.; Lin, P. S.; Schmidt-Ullrich, R.; Mikkelsen, R. B. Ionizing radiation-induced, mitochondria-dependent generation of reactive oxygen/nitrogen. *Cancer Res* **61**:3894-3901; 2001.

[15] Pham, N. A.; Hedley, D. W. Respiratory chain-generated oxidative stress following treatment of leukemic blasts with DNA-damaging agents. *Exp Cell Res* **264**:345-352; 2001.

[16] Murphy, M. P. How mitochondria produce reactive oxygen species. *Biochem J* **417**:1-13; 2009.

[17] de Moura, M. B.; dos Santos, L. S.; Van Houten, B. Mitochondrial dysfunction in neurodegenerative diseases and cancer. *Environ Mol Mutagen* **51**:391-405; 2010.

[18] Balaban, R. S.; Nemoto, S.; Finkel, T. Mitochondria, oxidants, and aging. *Cell* **120**:483-495; 2005.

[19] Jastroch, M.; Divakaruni, A. S.; Mookerjee, S.; Treberg, J. R.; Brand, M. D. Mitochondrial proton and electron leaks. *Essays Biochem* **47**:53-67; 2010.

[20] Kalyanaraman, B.; Darley-Usmar, V.; Davies, K. J.; Dennery, P. A.; Forman, H. J.; Grisham, M. B.; Mann, G. E.; Moore, K.; Roberts, L. J.; Ischiropoulos, H. Measuring reactive oxygen and nitrogen species with fluorescent probes: challenges and limitations. *Free Radic Biol Med* **52**:1-6; 2012.

[21] Gomes, A.; Fernandes, E.; Lima, J. L. Fluorescence probes used for detection of reactive oxygen species. *J Biochem Biophys*

Methods **65**:45-80; 2005.

[22] Cottet-Rousselle, C.; Ronot, X.; Leverve, X.; Mayol, J. F. Cytometric assessment of mitochondria using fluorescent probes. *Cytometry A* **79**:405-425; 2011.

[23] Kalyanaraman, B. Oxidative chemistry of fluorescent dyes: implications in the detection of reactive oxygen and nitrogen species. *Biochem Soc Trans* **39**:1221-1225; 2011.

[24] Pandian, R. P.; Kutala, V. K.; Parinandi, N. L.; Zweier, J. L.; Kuppusamy, P. Measurement of oxygen consumption in mouse aortic endothelial cells using a microparticulate oximetry probe. *Arch Biochem Biophys* **420**:169-175; 2003.

[25] Diepart, C.; Verrax, J.; Calderon, P. B.; Feron, O.; Jordan, B. F.; Gallez, B. Comparison of methods for measuring oxygen consumption in tumor cells in vitro. *Anal Biochem* **396**:250-256; 2010.

[26] Pandian, R. P.; Parinandi, N. L.; Ilangovan, G.; Zweier, J. L.; Kuppusamy, P. Novel particulate spin probe for targeted determination of oxygen in cells and tissues. *Free Radic Biol Med* **35**:1138-1148; 2003.

[27] Fujii, H.; Sakata, K.; Katsumata, Y.; Sato, R.; Kinouchi, M.; Someya, M.; Masunaga, S.; Hareyama, M.; Swartz, H. M.; Hirata, H. Tissue oxygenation in a murine SCC VII tumor after X-ray irradiation as determined by EPR spectroscopy. *Radiother Oncol* **86**:354-360; 2008.

[28] Remels, A. H.; Langen, R. C.; Schrauwen, P.; Schaart, G.; Schols, A. M.; Gosker, H. R. Regulation of mitochondrial biogenesis during myogenesis. *Mol Cell Endocrinol* **315:**113-120; 2010.

[29] Schreiber, S. N.; Emter, R.; Hock, M. B.; Knutti, D.; Cardenas, J.; Podvinec, M.; Oakeley, E. J.; Kralli, A. The estrogen-related receptor alpha (ERRalpha) functions in PPARgamma coactivator 1alpha (PGC-1alpha)-induced mitochondrial biogenesis. *Proc Natl Acad Sci U S A* **101:**6472-6477; 2004.

[30] Ljubicic, V.; Hood, D. A. Kinase-specific responsiveness to incremental contractile activity in skeletal muscle with low and high mitochondrial content. *Am J Physiol Endocrinol Metab* **295:**E195-204; 2008.

[31] Jahnke, V. E.; Sabido, O.; Freyssenet, D. Control of mitochondrial biogenesis, ROS level, and cytosolic Ca2+ concentration during the cell cycle and the onset of differentiation in L6E9 myoblasts. *Am J Physiol Cell Physiol* **296:**C1185-1194; 2009.

[32] Mitra, K.; Wunder, C.; Roysam, B.; Lin, G.; Lippincott-Schwartz, J. A hyperfused mitochondrial state achieved at G1-S regulates cyclin E buildup and entry into S phase. *Proc Natl Acad Sci U S A* **106:**11960-11965; 2009.

[33] Pawlik, T. M.; Keyomarsi, K. Role of cell cycle in

mediating sensitivity to radiotherapy. *Int J Radiat Oncol Biol Phys* **59**:928-942; 2004.

[34] Gong, B.; Chen, Q.; Almasan, A. Ionizing radiation stimulates mitochondrial gene expression and activity. *Radiat Res* **150**:505-512; 1998.

[35] Gudz, T. I.; Pandelova, I. G.; Novgorodov, S. A. Stimulation of respiration in rat thymocytes induced by ionizing radiation. *Radiat Res* **138**:114-120; 1994.

[36] Battino, M.; Ferri, E.; Gattavecchia, E.; Breccia, A.; Genova, M. L.; Littarru, G. P.; Lenaz, G. Mitochondrial respiratory chain features after gamma-irradiation. *Free Radic Res* **26**:431-438; 1997.

[37] Nugent, S.; Mothersill, C. E.; Seymour, C.; McClean, B.; Lyng, F. M.; Murphy, J. E. Altered mitochondrial function and genome frequency post exposure to γ-radiation and bystander factors. *Int J Radiat Biol* **86**:829-841; 2010.

[38] Indo, H. P.; Davidson, M.; Yen, H. C.; Suenaga, S.; Tomita, K.; Nishii, T.; Higuchi, M.; Koga, Y.; Ozawa, T.; Majima, H. J. Evidence of ROS generation by mitochondria in cells with impaired electron transport chain and mitochondrial DNA damage. *Mitochondrion* **7**:106-118; 2007.

[39] Kadenbach, B. Intrinsic and extrinsic uncoupling of oxidative phosphorylation. *Biochim Biophys Acta* **1604**:77-94; 2003.

[40] Korshunov, S. S.; Skulachev, V. P.; Starkov, A. A. High protonic potential actuates a mechanism of production of reactive oxygen species in mitochondria. *FEBS Lett* **416**:15-18; 1997.

[41] Piacentini, M.; Farrace, M. G.; Piredda, L.; Matarrese, P.; Ciccosanti, F.; Falasca, L.; Rodolfo, C.; Giammarioli, A. M.; Verderio, E.; Griffin, M.; Malorni, W. Transglutaminase overexpression sensitizes neuronal cell lines to apoptosis by increasing mitochondrial membrane potential and cellular oxidative stress. *J Neurochem* **81**:1061-1072; 2002.

[42] Gergely, P.; Niland, B.; Gonchoroff, N.; Pullmann, R.; Phillips, P. E.; Perl, A. Persistent mitochondrial hyperpolarization, increased reactive oxygen intermediate production, and cytoplasmic alkalinization characterize altered IL-10 signaling in patients with systemic lupus erythematosus. *J Immunol* **169**:1092-1101; 2002.

[43] Nugent, S. M.; Mothersill, C. E.; Seymour, C.; McClean, B.; Lyng, F. M.; Murphy, J. E. Increased mitochondrial mass in cells with functionally compromised mitochondria after exposure to both direct gamma radiation and bystander factors. *Radiat Res* **168**:134-142; 2007.

[44] Malakhova, L.; Bezlepkin, V. G.; Antipova, V.; Ushakova, T.; Fomenko, L.; Sirota, N.; Gaziev, A. I. The increase in mitochondrial DNA copy number in the tissues of

gamma-irradiated mice. *Cell Mol Biol Lett* **10**:721-732; 2005.

[45] Havens, C. G.; Ho, A.; Yoshioka, N.; Dowdy, S. F. Regulation of late G1/S phase transition and APC Cdh1 by reactive oxygen species. *Mol Cell Biol* **26**:4701-4711; 2006.

[46] Martínez-Diez, M.; Santamaría, G.; Ortega, A. D.; Cuezva, J. M. Biogenesis and dynamics of mitochondria during the cell cycle: significance of 3'UTRs. *PLoS One* **1**:e107; 2006.

[47] Kobashigawa, S.; Suzuki, K.; Yamashita, S. Ionizing radiation accelerates Drp1-dependent mitochondrial fission, which involves delayed mitochondrial reactive oxygen species production in normal human fibroblast-like cells. *Biochem Biophys Res Commun* **414**:795-800; 2011.

[48] Hall, E. J.; Giaccia, A. J. *Radiobiology for the radiologist.* Lippincott Williams & Wilkins; 2006.

[49] Busse, P. M.; Bose, S. K.; Jones, R. W.; Tolmach, L. J. The action of caffeine on X-irradiated HeLa cells. III. Enhancement of X-ray-induced killing during G2 arrest. *Radiat Res* **76**:292-307; 1978.

Figure Legends

Fig. 1. Flow cytometric analysis of cellular oxidative stress levels and mitochondrial ROS levels in A549 cells after Ir. (A and B) Cellular oxidative stress levels measured by DCFDA. (A) Representative flow cytometric profiles obtained from the cells after 0 and 12 h after Ir. (B) Time course of the relative cellular oxidative stress levels. (C and D) Mitochondrial ROS levels measured by MSR. (C) Representative flow cytometric profiles obtained from the cells after 0 and 12 h after Ir. (D) Time course of the relative mitochondrial ROS levels. Data are expressed as means ± SE of three experiments. *p < 0.05; **p < 0.01 vs. 0 h (Student's *t*-test).

Fig. 2. Flow cytometric analysis of mitochondrial membrane potential in A549 cells after Ir. (A) Representative flow cytometric profiles obtained from the cells after 0 and 12 h after Ir. (B) Time course of the relative membrane potential. Data are expressed as means ± SE of four experiments. *p < 0.05; **p < 0.01 vs. 0 h (Student's *t*-test). (C) Effect of CCCP on mitochondrial membrane potential. Data are expressed as means ± SE of three experiments. *p < 0.05 (Student's *t*-test).

Fig. 3. Oxygen consumption in A549 cells after Ir measured by polarography. (A) Representative polarograph traces. The

oxygen concentration was monitored in the presence (0 h and 12 h) and absence (buffer only) of cells. Rotenone (2 μM) was added to stop mitochondrial respiration. (B) Oxygen consumption rate in A549 cells after Ir. Data are expressed as means ± SE of three experiments. *p < 0.05 (Student's *t*-test).

Fig. 4. Oxygen consumption in A549 cells after Ir measured by ESR oxymetry. (A) Representative ESR spectra obtained from non-irradiated (left) or irradiated (right) A549 cells. (B) Changes in pO_2 in A549 cells after Ir. After irradiation, A549 cells were incubated for 0 (●), 6 (○), 12 (■), or 24 (□) hours, followed by the ESR measurements. Representative plots of three experiments are shown. (C) Oxygen consumption rates in A549 cells after Ir. Data are expressed as means ± SE of three experiments. *p < 0.05 vs. 0 h (Student's *t*-test). (D) Effect of rotenone on changes in pO_2 in A549 cells with and without Ir exposure. Representative plots of three experiments are shown. ●; Ir(-)/rotenone(-), ■; Ir(-)/rotenone(+), ○; Ir(+)/rotenone(-), □; Ir(+)/rotenone(+). (E) Effect of rotenone on cellular oxygen consumption. Data are expressed as means ± SE of three experiments. *p < 0.05; **p < 0.01 (Student's *t*-test).

Fig. 5. Cellular ATP content in A549 cells after Ir. (A) Time

course of the relative cellular ATP content. After 10 Gy irradiation, A549 cells were collected and cellular ATP content was measured as described in the text. The ATP amounts at each time point were normalized to the ATP amount at 0 h after Ir. (B) Effect of oligomycin on cellular ATP content after Ir. Immediately after irradiation, A549 cells were incubated with oligomycin for 12 h. The ATP amounts in each condition were normalized to the ATP amount obtained from Ir(-)/oligomycin(-) cells. Data are expressed as means ± SE of four experiments. *p < 0.05 vs. 0 h (Student's *t*-test).

Fig. 6. Effect of the complex II inhibitor 3-nitropropionic acid (3-NP) on mitochondrial ROS level after Ir. After A549 cells were X-irradiated, the cells were incubated with 3-NP at the indicated concentrations for 12 h. Intensities of MSR fluorescence in each condition were normalized to those obtained from Ir(-)/3-NP(-) cells. Data are expressed as means ± SE of three experiments.

Fig. 7. Mitochondrial content in A549 cells after Ir. (A) Mitochondrial mass measured by MitoTracker Green staining. After 10 Gy irradiation, A549 cells were stained with MitoTracker Green and analyzed using a flow cytometer. Representative flow cytometric profiles of three experiments

are shown. (B) Mitochondrial DNA (mtDNA) content measured by quantitative PCR. The relative amounts of D-loop and cytochrome c oxidase subunit II (COXII) in total DNA were determined as described in the text. MtDNA content at each time point was normalized to that at 0 h after Ir. Data are expressed as means ± SE of three experiments. *$p < 0.05$ vs. 0 h (Student's *t*-test).

Fig. 8. Simultaneous flow cytometric analysis of cell cycle/mitochondrial mass in A549 cells after Ir. After 10 Gy irradiation, A549 cells were double-stained with Nuclear-ID Red and MitoTracker Green, followed by the flow cytometric analysis. (A) Representative flow cytometric profiles in A549 cells after Ir analyzed by Nuclear-ID Red fluorescence.(B) MitoTracker Green fluorescence of the cell fraction corresponding to the G1, S, and G2/M phases. Representative flow cytometric profiles of MitoTracker Green fluorescence from each cell cycle fraction at the indicated times after Ir are overlaid and shown. white; G1, black; S, gray; G2/M.(C) Relative mitochondrial content during the cell cycle after Ir. Data are expressed as means ± SE of three experiments. **$p < 0.01$ vs. 0 h (Student's *t*-test).

Fig. 9. Simultaneous flow cytometric analysis of cell cycle/cellular oxidative stress levels in A549 cells after Ir. After 10 Gy irradiation, A549 cells were double-stained with

Nuclear-ID Red and DCFDA, followed by the flow cytometric analysis. (A) Representative flow cytometric profiles in A549 cells after Ir analyzed by Nuclear-ID Red fluorescence. (B) DCFDA fluorescence of the cell fraction corresponding to the G1, S, and G2/M phases. Representative flow cytometric profiles of DCFDA fluorescence from each cell cycle fraction at the indicated times after Ir are overlaid and shown. white; G1, black; S, gray; G2/M. (C) Relative cellular oxidative stress levels during the cell cycle after Ir. Data are expressed as means ± SE of three experiments. **p < 0.01 vs. 0 h (Student's *t*-test).

Table 1

Mitochondrial ETC enzyme activities after Ir

Condition	Complex I+III	Complex II+III	Complex IV	Complex I	Complex II
Ir (-)	27.8 ± 6.4	58.5 ± 10.5	228.8 ± 65.5	23.8 ± 4.3	38.7 ± 8.1
Ir (+)	26.3 ± 3.3	74.5 ± 15.8	216.1 ± 63.2	23.8 ± 8.4	61.8 ± 16.8

Complex I+III, complex II+III, and complex IV activities are expressed in nmol cytochrome c (reduced or oxidized)/min・mg protein. Complex I activities are expressed in nmol NADH/min・mg protein. Complex II activities are expressed in nmol DCPIP/min・mg protein. Data are expressed as means ± SE of at least five experiments.

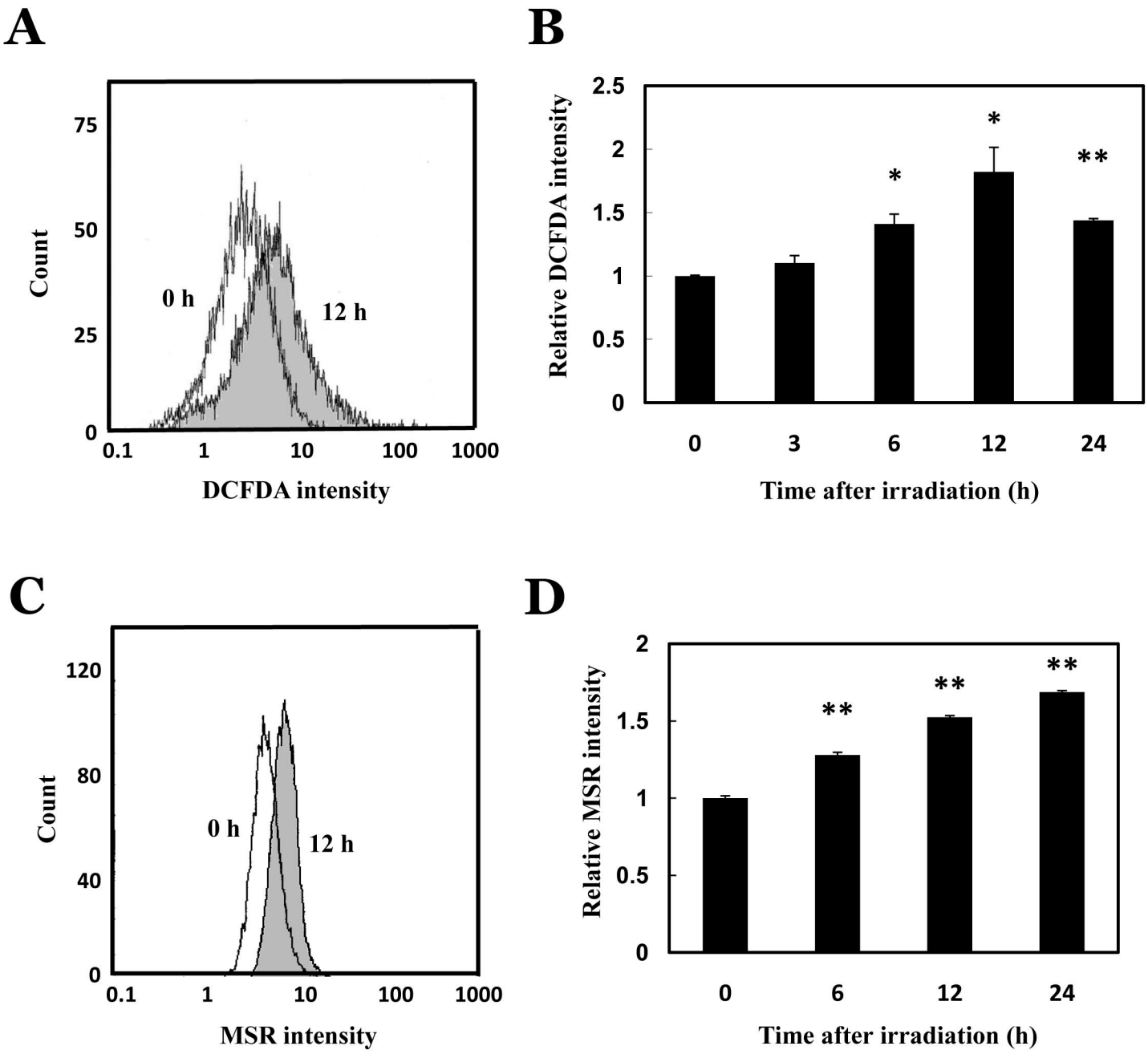

Fig. 1 Yamamori *et al.*

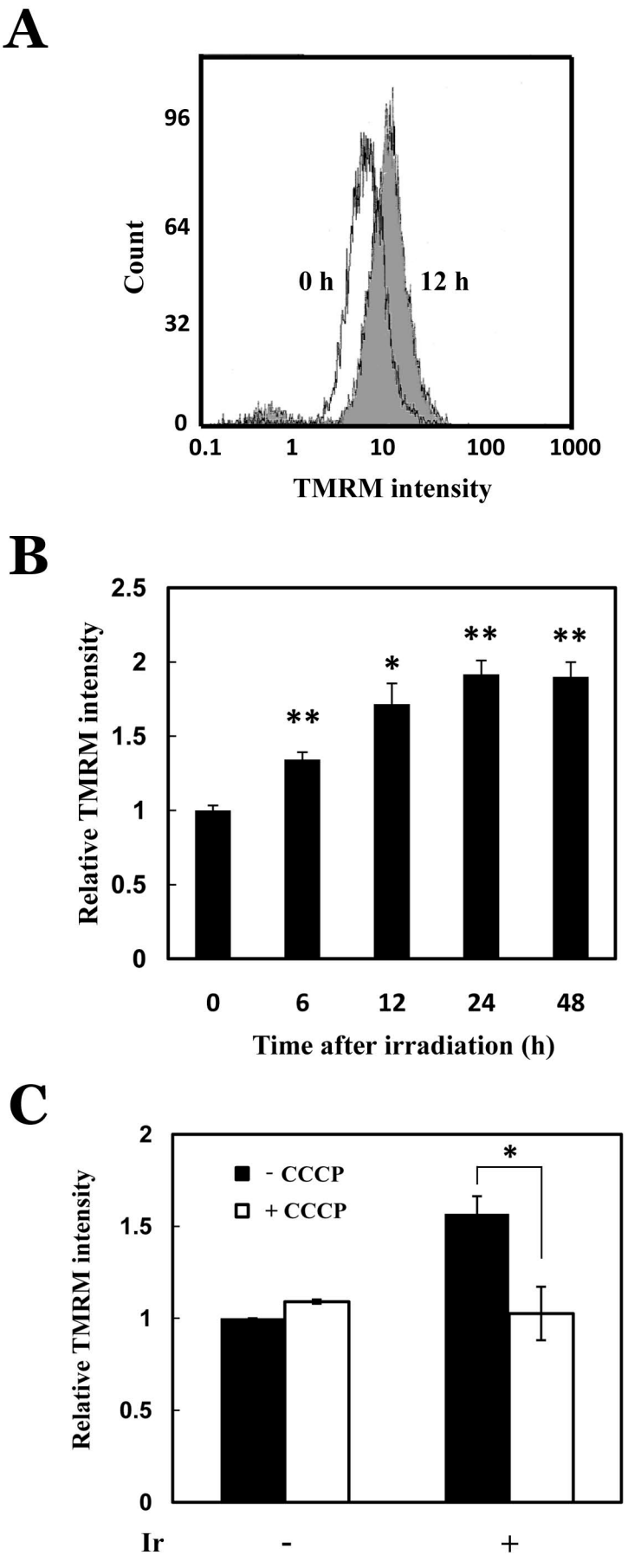

Fig. 2 Yamamori *et al.*

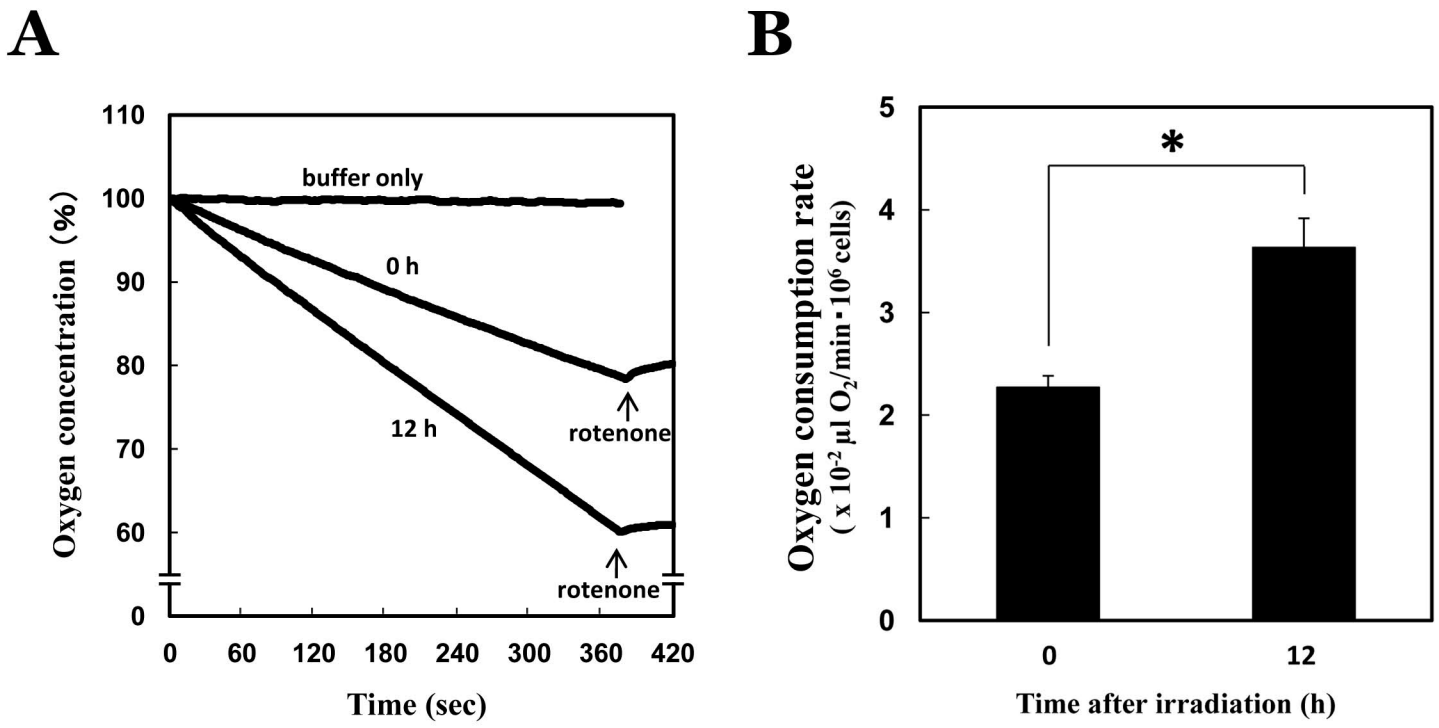

Fig. 3 Yamamori *et al.*

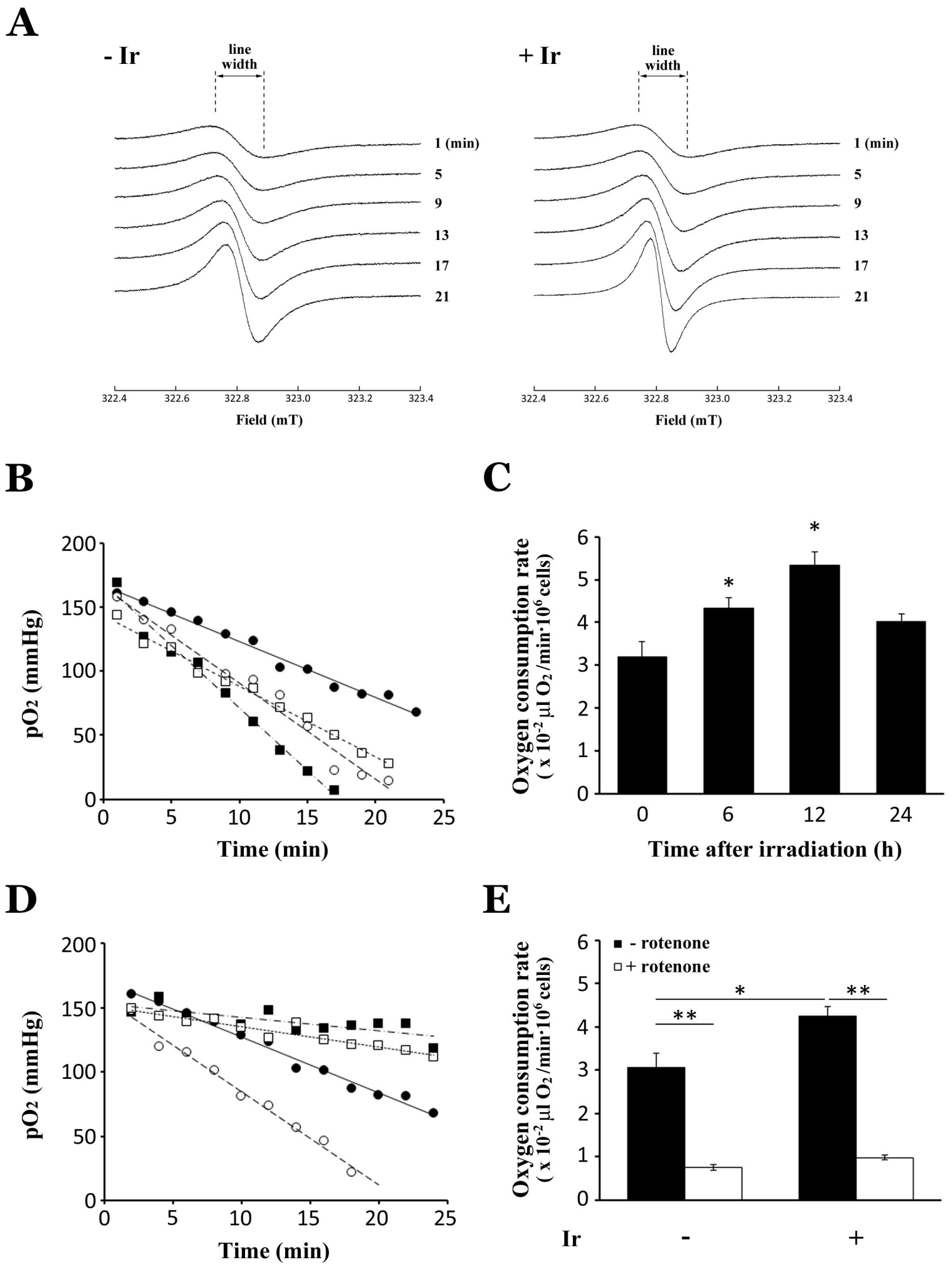

Fig. 4 Yamamori *et al.*

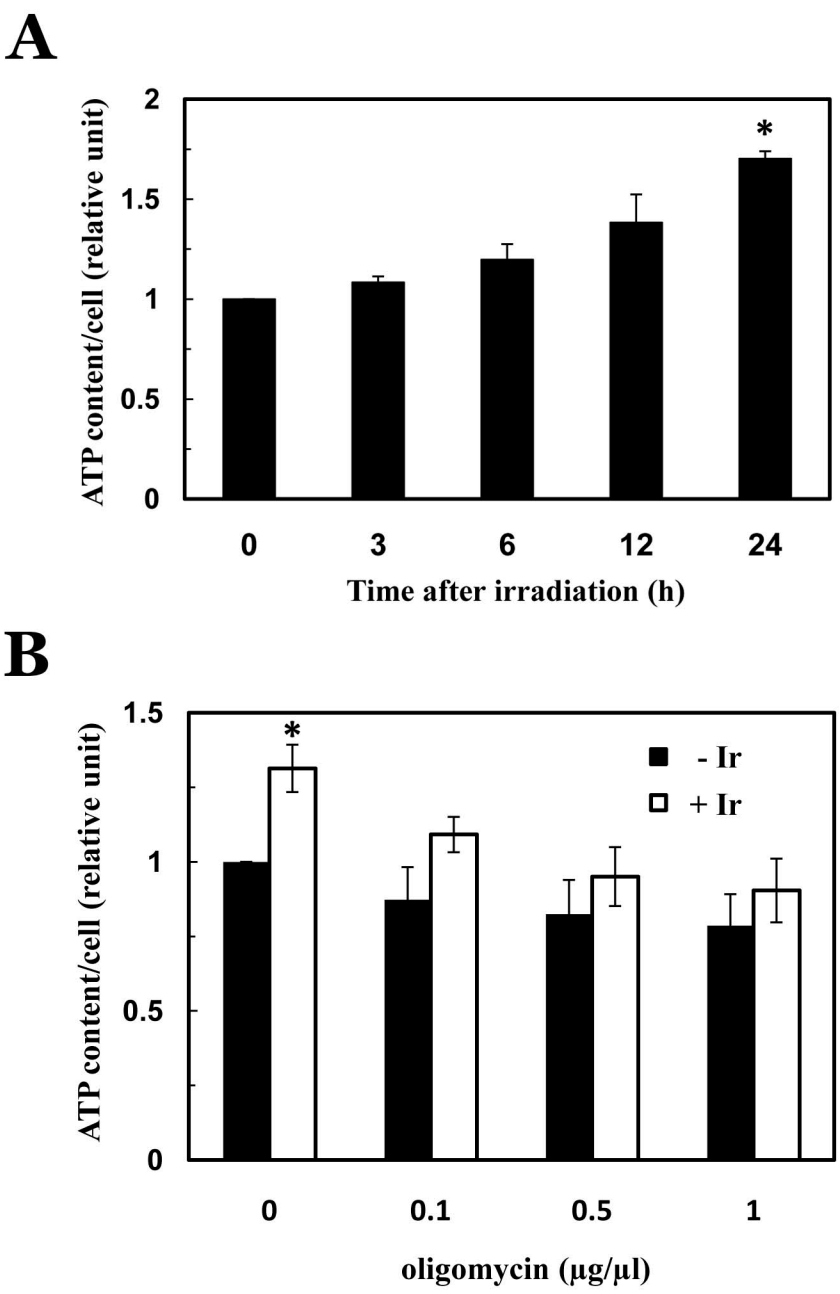

Fig. 5 Yamamori *et al.*

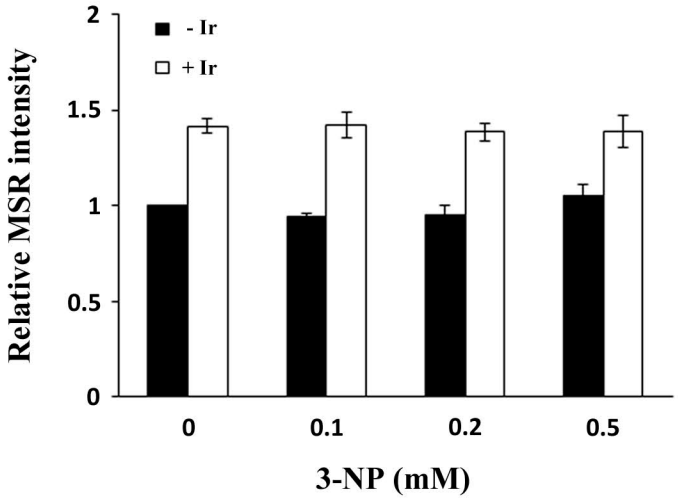

Fig. 6 Yamamori *et al.*

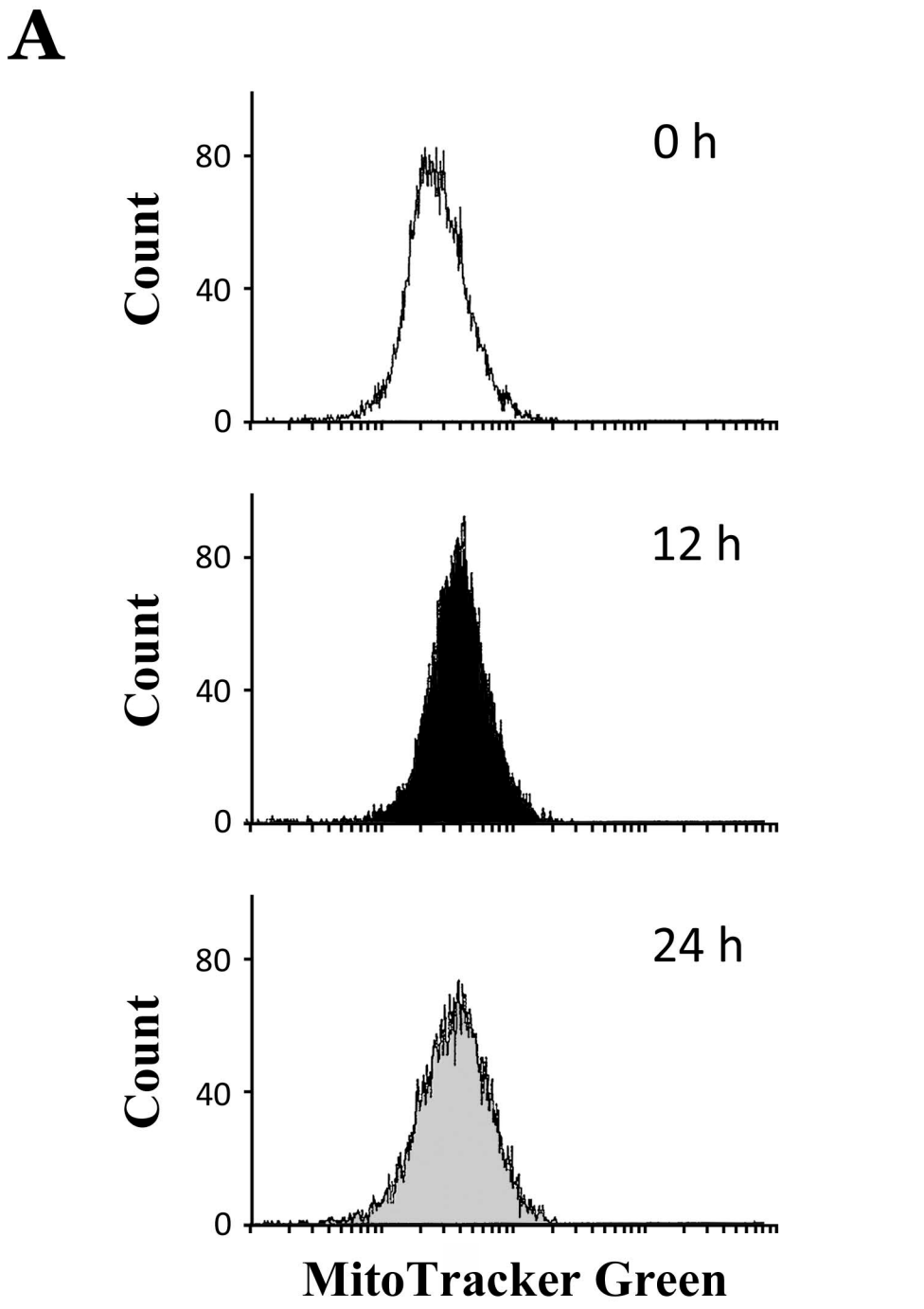

Fig. 7 Yamamori *et al.*

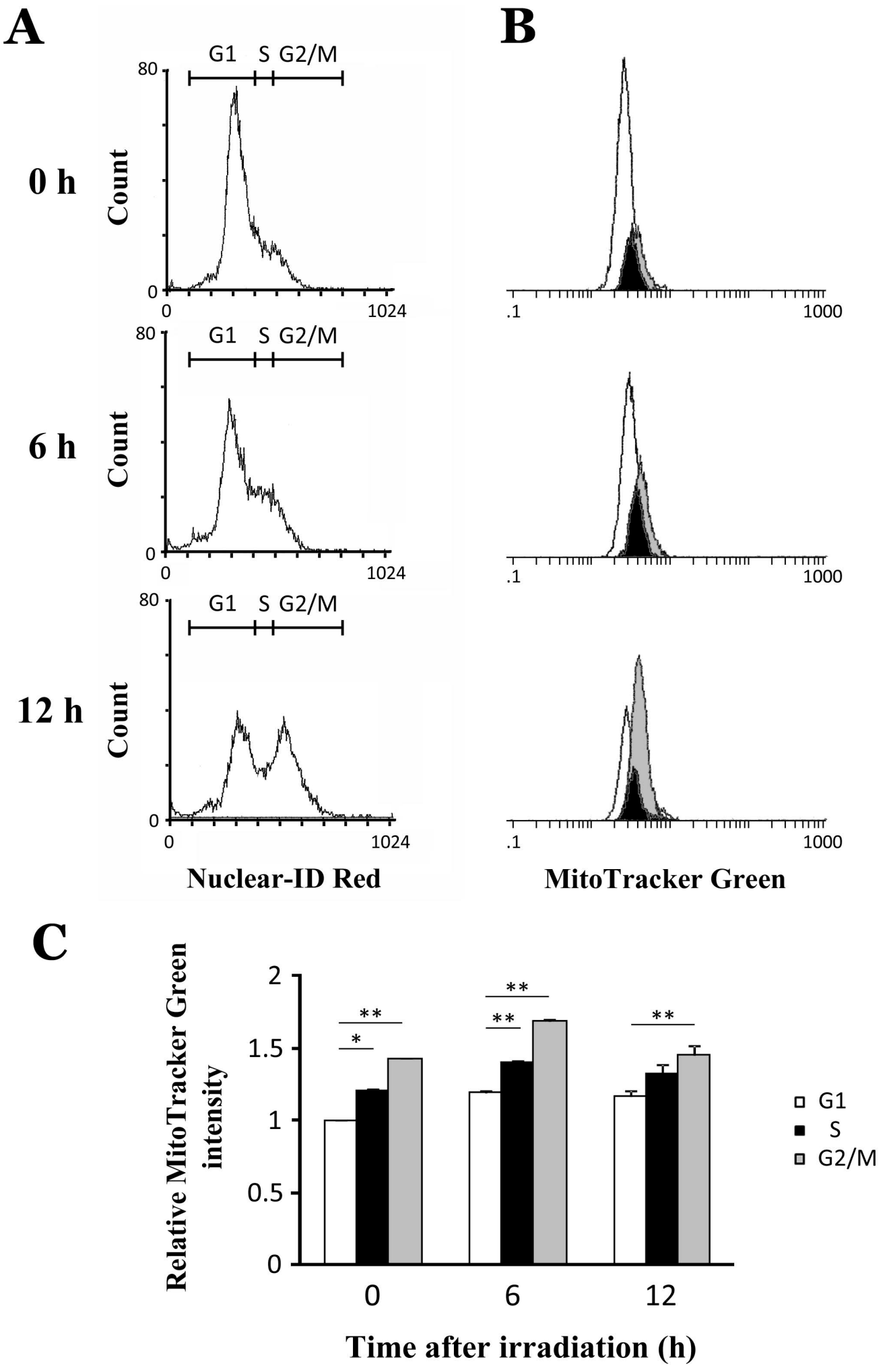

Fig. 8 Yamamori *et al.*

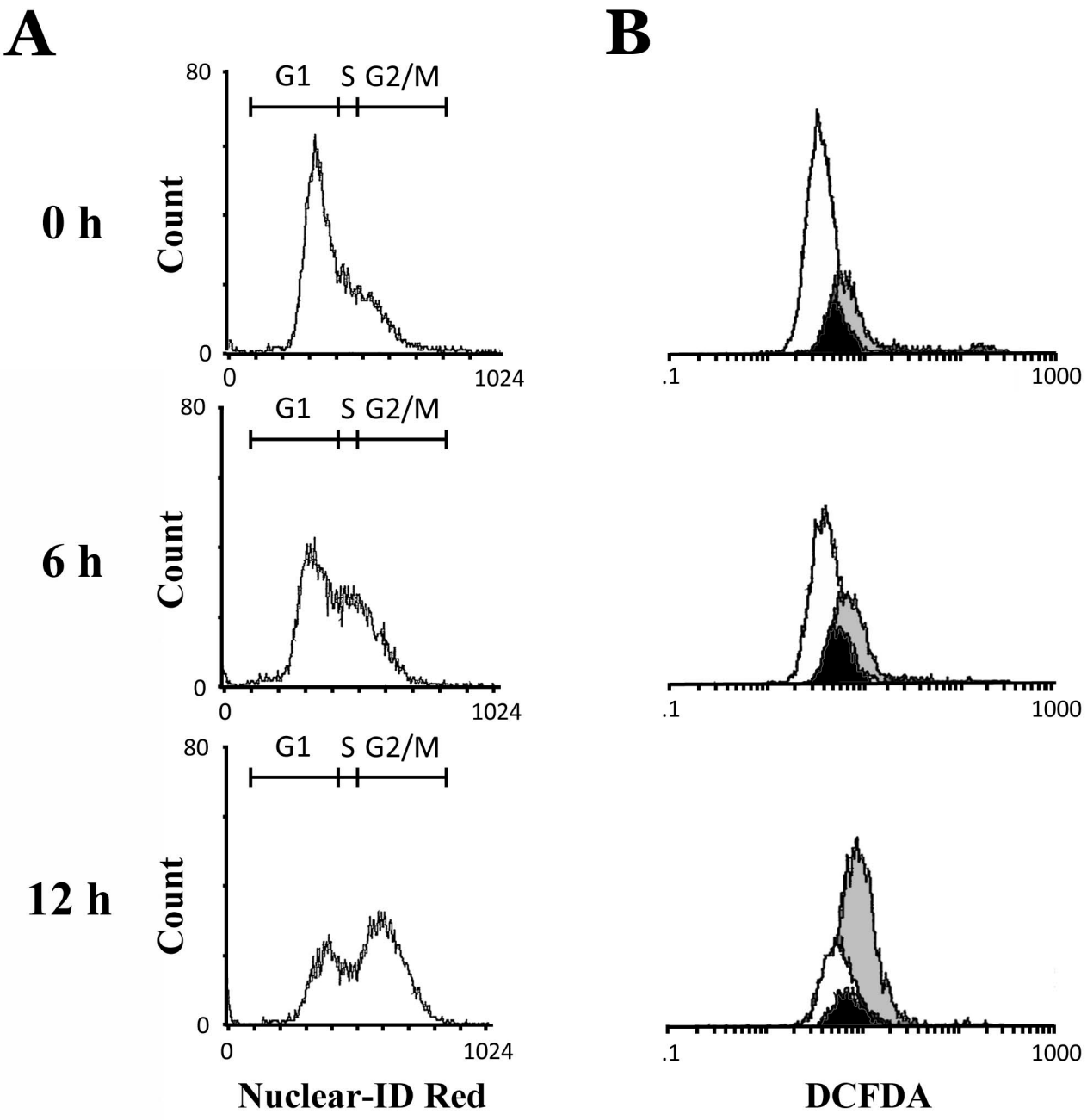

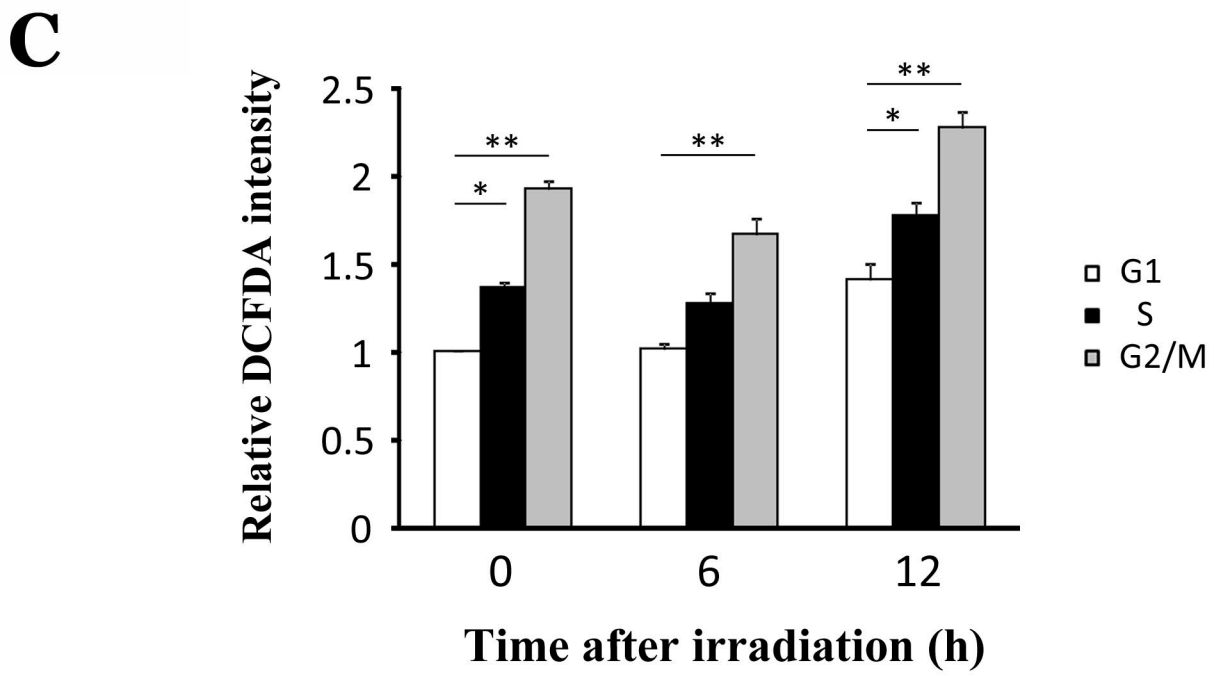

Fig. 9 Yamamori *et al.*